Gerd Buntkowsky*, Sonja Döller, Nadia Haro-Mares, Torsten Gutmann and Markus Hoffmann

Solid-state NMR studies of non-ionic surfactants confined in mesoporous silica

https://doi.org/10.1515/zpch-2021-3132
Received September 20, 2021; accepted October 12, 2021; published online October 27, 2021

Abstract: This review gives an overview of current trends in the investigation of confined molecules such as higher alcohols, ethylene glycol and polyethylene glycol as guest molecules in neat and functionalized mesoporous silica materials. All these molecules have both hydrophobic and hydrophilic parts. They are characteristic role-models for the investigation of confined surfactants. Their properties are studied by a combination of solid-state NMR and relaxometry with other physicochemical techniques and molecular dynamics techniques. It is shown that this combination delivers unique insights into the structure, arrangement, dynamical properties and the guest-host interactions inside the confinement.

Keywords: confinement; dynamic nuclear polarization (DNP); green solvents; host-guest interactions; solid-state NMR; surfactants.

1 Introduction

Organic solvents are produced and employed on the billion-ton scale for applications in industrial fine chemistry and pharmacy for reaction and product isolation processes. Many of these solvents are major environmental, security or

---

Dedicated to Paul Heitjans on the occasion of his 75th birthday.

***Corresponding author: Gerd Buntkowsky,** Eduard-Zintl-Institut für Anorganische und Physikalische Chemie, Technische Universität Darmstadt, Alarich-Weiss-Str. 8, D-64287 Darmstadt, Germany, E-mail: gerd.buntkowsky@chemie.tu-darmstadt.de
Sonja Döller, Nadia Haro-Mares and Torsten Gutmann, Eduard-Zintl-Institut für Anorganische und Physikalische Chemie, Technische Universität Darmstadt, Alarich-Weiss-Str. 8, D-64287 Darmstadt, Germany
Markus Hoffmann, Department of Chemistry and Biochemistry, State University of New York College at Brockport, Brockport, NY, 14420, USA

health hazards, owing to their toxicity, volatility, or flammability. One of the most important principles of Green Chemistry [1] is their replacement by innocuous environmentally benign solvents [1]. One of the most promising class of neoteric solvents is based on polyethylene glycol (PEG, Scheme 1(a)) [2–4]. PEGs are very attractive alternative solvents because they possess a negligible vapor pressure, are nontoxic, biodegradable, and inexpensively available as they are produced in industrial quantities. Owing to these favorable properties they are increasingly employed as media for synthetic organic chemistry, such as e.g. solvents in heterogeneously catalyzed reactions where the transition metal catalyst is immobilized on a solid material of large surface area [4]. These transition metal catalysts are typically used for the important class of cross coupling reactions [5, 6]. For example, the Heck reaction of aryl halides and olefins was successfully carried out in PEG 400 (400 reflects the average molar weight of 400 g/mol) using as catalyst Pd immobilized onto mesoporous silica by 3-aminopropyltriethoxysilane (APTES) and vanillin as linker molecules [7].

An important factor for technical applications of catalysts immobilized in mesoporous support materials is the presence of confinement effects in dependence of the pore size. It is well-known that many small molecules exhibit very different physicochemical properties in confinement compared to their bulk phase, as has been discussed in a number of recent reviews and original papers cited therein [8–10]. As a prominent recent example, Fumagalli et al. [11] have found that the dielectric constant of water drastically reduces under confinement. Thus, there is a pressing need of fundamentally understanding the role of PEG as a solvent in heterogeneous catalysis, as well as a need to understand confinement effects of PEG and other molecules residing in pore structures relevant for immobilized transition metal catalysts. Carvalho et al. [12] have shown that PEG-related nonionic surfactants of the type C_mE_n or $C_mE_nP_q$ (see Scheme 1)

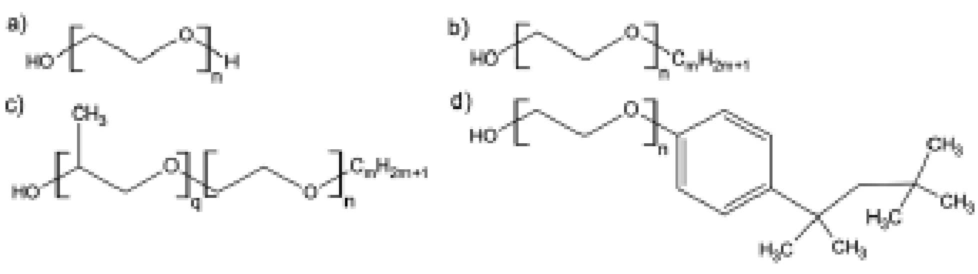

Scheme 1: Chemical structures of typical surfactants: (a) polyethylene glycol (PEG) with ethylene glycol for $n = 1$, (b) linear alkyl polyethylene oxide alcohol typically abbreviated by the notation C_mE_n, (c) branched alkyl polyethylene oxide, iso-propylene oxide alcohol abbreviated as $C_mE_nP_q$, (d) Triton X-100.

possess similar physical and environmentally benign characteristics and Hoffmann et al. [13] demonstrated as a proof of principle that the Diels–Alder reaction can be successfully carried out in C_6E_{10} as solvent. Moreover C_mE_n and $C_mE_nP_q$ type surfactants are widely used as structure directing templates in synthesis of nanomaterials [14], self-assembly processes to mimic biological systems [15], or adsorbents of toxic aromatic hydrocarbons and pesticides [16].

In the present review the focus is set to porous silica materials. Together with the related porous alumosilicates, they form the most important and versatile class of micro- and mesoporous solid host-systems materials, spanning a diameter range from fractions of a nanometer to ca. 50 nm and above. Typical members of this class are microporous zeolites, and mesoporous materials such as periodical mesoporous silica (PMS) [17, 18], controlled porous glasses and aerogels. The mesoporous materials opened up new research fields, as they allowed to introduce larger molecular entities into well-defined pores as the conventional zeolites with their characteristic narrow pore diameters.

In particular, PMS-type materials are ideal solid host-systems, which can be easily handled under ambient conditions (room temperature under air), owing to their good chemical stability. They exhibit narrow pore-diameter distributions, which are adjustable by their preparation. They have large specific surface areas and volumes. The large density of surface silanol (Si-OH) groups on these PMS materials permits the easy chemical modification or functionalization of their surfaces. Employing suitable linker molecules, it is e.g. possible to control the polarity, the hydrophilicity, the hydrogen bonding, or the catalytic properties of the surface. By tethering amide or carboxy function groups [19] to the silanol groups on the porous silica surface via linker molecules, it is possible to bind various types of chemical functions by post-synthetic grafting in a second step. In some favorable cases, it is also possible to obtain such surface modified porous materials directly during their synthesis by employing co-condensation reactions with suitably functionalized reactant molecules [20, 21]. Owing to their favorable application properties, PMS were employed as hosts in confinement studies of diverse molecules as water, alcohols, carbonic acids, and protein solutions [22–28] or in electrochemical studies of local pK_a values in confinement [29]. The most prominent PMS materials with about 10,000 references in the web of science in article titles are Mobil Composition of Matter No. 41 (MCM-41) [30], Santa Barbara Amorphous (SBA-15) [31, 32], and their various derivates. They are all characterized by well-defined hexagonally arranged pore arrays. Other important members of the family with three dimensional sponge like pore structures are mesoporous glasses such as Vycor [33] or CPG-10-75 [34, 35]. They are applied in separation techniques, in heterogeneous catalysis, in drug delivery, in gas-storage and many other fields.

In order to understand the properties of molecules confined in the mesopores, a thorough characterization of the host–guest and guest–guest interactions by a combination of various complementary experimental and computational techniques is necessary. Nitrogen adsorption reveals the specific surface areas, pore volumes and pore diameters [36, 37]. Diffractometry techniques such as powder X-ray diffraction (PXRD) as well as small angle X-ray and neutron scattering (SAXS and SANS) monitor the ordering of the material [38–40]. NMR techniques including multi-nuclear, variable-temperature, solid-state NMR (SSNMR) reveal the local ordering and dynamics on the molecular level. Differential scanning calorimetry (DSC) and thermogravimetric analysis (TGA) yield information on phase transitions and desorption processes inside the pores. Finally, theoretical calculations including Molecular Dynamics (MD) simulations often provide the needed molecular level insights to allow for a proper qualitative and quantitative interpretation of the experimental results [41, 42].

In the present short review recent results on the investigation of non-ionic surfactants confined in mesoporous host systems by the application of normal and Dynamic Nuclear Polarization (DNP) enhanced solid-state NMR techniques are discussed. A detailed introduction into SSNMR techniques of porous systems is beyond the scope of this review and can be found in a number of reviews [43–46]. For a detailed discussion of DNP the reader is referred to the recent review by Corzilius et al. [47], Lafon et al. [48] and the original references cited in these reviews. The background of melting and glass transitions in confinement is found in refs. [26, 49–51] and references cited therein.

SSNMR techniques do not depend on local or global ordering of the system under investigation [52], and are therefore complementary structure analyses tools to diffractometry. In addition, they can monitor not only structural but also dynamical processes, such as e.g. phase transitions [41, 42]. Their drawback is their low sensitivity, which necessitates relatively large amounts of probe molecules. In the case of confinement or surface studies, this is equivalent with high specific volumes and specific surface areas.

Thus, most SSNMR studies employ microporous materials like zeolites [53–57] or mesoporous materials like MCM-41 and SBA-15 and their derivatives [58–61]. SSNMR is particularly powerful for the characterization of surface functionalized systems [62–64], and the monitoring of surface reactions such as catalytic transformation of epoxides under CO_2 atmosphere on silica-supported aminopyridinium halides [65], the tethering of linkers [66], or the silylation of amorphous silica materials [67]. Other examples are the investigation of inhibitory processes in aldol reactions in amine-functionalized silica supports [68, 69], or the study of the dynamics of grafted molecules as a function of the temperature and water content inside the pores [70–72]. Coperet et al. [73–83] investigated a series of supported organometallic catalysts by SSNMR. Pruski et al. [84–94] and Buntkowsky et al. [95–105] employed SSNMR for the characterization of immobilized molecules [106–109]; and Klimavicius et al. [110] for the study of confined ionic liquids. Recently it was realized that mesoporous silica materials have also a substantial potential in the optimization of Li-ion batteries [111]. Here it would be of great interest to employ the dynamic solid-state NMR techniques pioneered by Heitjans et al. [112–115] to characterize these systems.

While these examples clearly demonstrate the power of SSNMR to characterize these host materials and their confined guests, they are all performed on large specific surface materials, owing to the sensitivity problem of SSNMR. While it is possible to slightly meliorate this problem for SSNMR of X-nuclei by indirect detection via ^{1}H under magic angle spinning (MAS) [116], as shown by Pruski et al. in a series of papers [85–87, 89], the most powerful remedy of the drawback is sensitivity enhancement with hyperpolarization techniques such as Dynamic Nuclear Polarization (DNP) [117–120], Surface Enhanced NMR Spectroscopy (SENS) [76, 77, 79, 82, 121–127], Parahydrogen Induced Polarization (PHIP) [128–134], and spin-exchange optical pumping (SEOP) [135, 136].

While the focus of this review is devoted to results obtained by our group in the last years, there are also short reports about important contributions from other groups. The rest of this review is organized as follows: Section two gives an introduction into the preparation and surface modification of the mesoporous host materials. Section three discusses the behavior of confined surfactants and section four discusses some important aspects of DNP enhanced SSNMR in these systems. The review is finished by a summary and an outlook into possible future developments of the field.

2 Mesoporous silica materials for confinement studies

Initially, zeolites were the most prominent host materials. They are employed in heterogeneous catalysis [137, 138], gas storage [139], water purification and ion exchange [140], as molecular sieves [141, 142] and in many other applications. Owing to their microporous nature with narrow pore diameters below 1 nm, they are

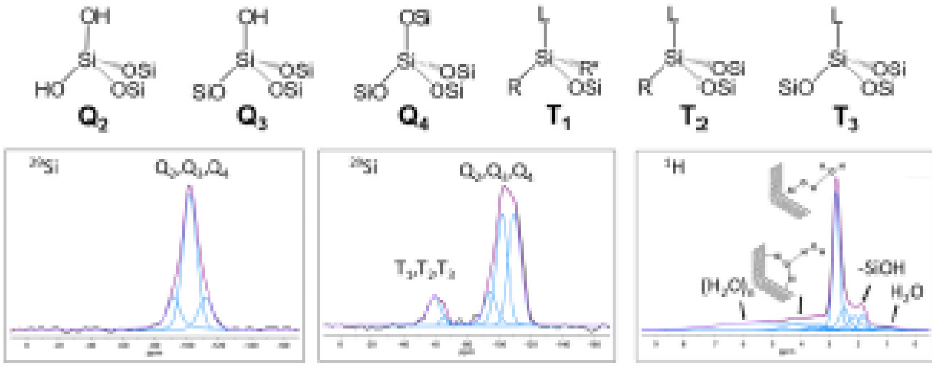

Figure 1: SSNMR of APTES functionalization of MCM-41 materials with specific pore volume of 0.77 cm^3/g, specific surface area of 1000 m^2/g and a specific pore diameter of 3.6 nm. Upper row: chemical structures of the surface silica groups before (Q_n) and after (T_n) functionalization with APTES (L = propylamine. R,R* = –OEt or –OH). Lower row: ^{29}Si CPMAS (10 kHz) spectra of neat (left) and functionalized (center) silica (adapted from Weigler et al. [145]), and ^{1}H MAS spectrum of a non-dried MCM-41 at 10 kHz (black) (assignment according to Grünberg et al. [146]).

To solve this problem, mesoporous silica materials like MCM-41 or SBA-15 with larger and adjustable (via the preparation) pore sizes were developed. They combine large specific volumes and specific surface areas with high thermal stability, low specific weights and narrow pore diameter distributions [147–150]. Both types of materials are relatively easy to prepare and to functionalize, following e.g. the synthesis protocol by Grünberg et al. [64] or Grün et al. [151] (for details see refs. [148, 152]). In many confinement applications a detailed knowledge of the pore and surface parameters is necessary, which can be obtained by the combination of nitrogen adsorption (BET and BJH) and ^{29}Si SSNMR spectroscopy. Figure 1 displays the ^{29}Si-NMR characteristic of the surface silica groups of a functionalized silica after synthesis and after functionalization with APTES. The success of the functionalization is revealed by the change from Q_n silica surface groups (neat surface) to T_n functionalized silica surface groups when the subscript n expresses the number of OSi bonded to the silicon atom.

Most freshly prepared samples contain a substantial amount of surface bound water molecules [52, 146, 153], which in general have to be removed for confinement studies employing special drying protocols for the preparation of "water-free" silica samples [154].

3 NMR of confined surfactants

In this section, the behavior of octanol and isobutyric acid, which are suitable model compounds for larger, more complex surfactants are shortly reviewed. A special emphasis in these studies was the comparison of the neat liquid with liquid solutions of two or more liquid components [155]. The latter are of particular interest as they are models for many natural or technical systems, such as e.g. natural membranes.

3.1 Water-octanol mixtures

Water-octanol mixtures are the standard reference system for the characterization of the phase behavior of two immiscible liquids, and are employed to define the water octanol partition coefficient or p-value K_{ow} [156]. Liquids with high K_{ow} are hydrophobic and liquids with low K_{ow} are hydrophilic. K_{ow}-values are important to e.g. estimate the properties of oil/water mixtures in ecological systems or for estimating the distribution of drugs within the body in pharmacology [157]. Figure 2 displays the results of an experimental SSNMR study of

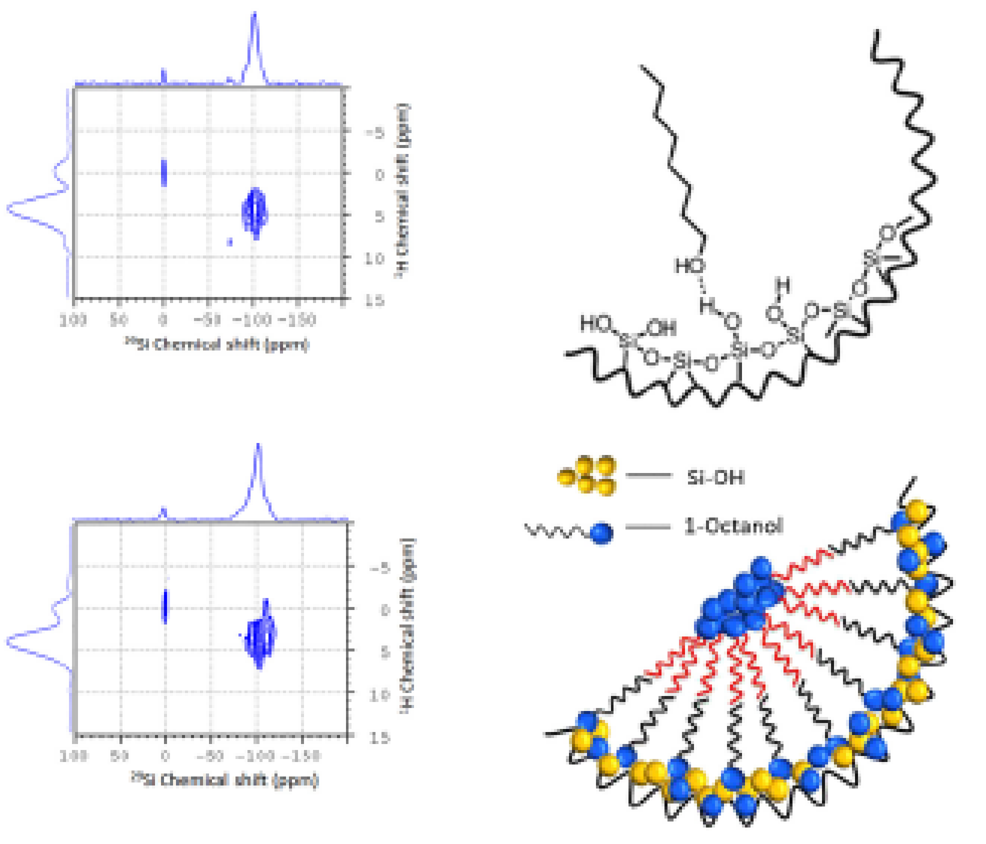

Figure 2: Left: 8 kHz ^{1}H–^{29}Si CPMAS FSLG-HETCOR spectra measured at room temperature of dried SBA-15 filled with a mixture of 80:20 mol % of 1-octanol and water at contact times of 3 ms (upper spectrum) and 9 ms (lower spectrum). Right: hydrogen bonding interactions between silanol and hydroxy groups cause ordering of the octanol molecules on the surface (upper figure). This ordering is transmitted via hydrophilic interactions inside the pores, resulting in a double-layered cylindrical model of the confined octanol (for details see Kumari et al. [159]).

water/octanol mixtures confined in mesoporous SBA-15. Employing a combination of 1D ^{1}H-MAS NMR, ^{29}Si-CPMAS (Cross-Polarization Magic Angle Spinning) NMR, and ^{1}H/^{29}Si-HETCOR (Heteronuclear Correlation) experiments, obtained by Frequency Switched Lee–Goldburg (FSLG)-NMR [158], it is possible to assign and estimate the strength of the magnetic dipolar interactions between the different components and thus determine the distributions of the two liquids inside the confinement [159]. Effects of the sample spinning on the confined liquids can be neglected at the employed spinning frequencies.

3.2 Water-isobutyric acid mixtures

In contrast to the water/octanol system discussed in the previous section, where the bulk phase diagram contains a large miscibility gap, bulk water/isobutyric acid (iBA, 2-methylpropanoic acid) solutions are completely miscible above a mole fraction dependent critical temperature. Below this temperature they phase-separate into a water and an iBA rich fraction. This property makes water/iBA systems ideal models for the investigation of micro-phase separation processes in confinement by NMR. A combination of ^{1}H-diffusometry and ^{1}H-relaxometry revealed an anomalous temperature dependence of the self-diffusion coefficient and a bifurcation of the T_2-relaxation upon a critical temperature of 42 °C [52, 160, 161]. Based on these data, a structural model in the form of concentric cylindrical liquid layers inside the pores was proposed for temperatures below the critical temperature. This model was later refined by a combination of ^{1}H–^{29}Si FSLG HETCOR (Figure 3, upper panel) and MD simulations on frozen solutions (110 K) of iBA/H_2O mixtures confined in SBA-15 [162]. At low temperatures, the molecular dynamics of the confined molecules are so slow that dipolar interactions can be revealed in the HETCOR in the form of cross-peaks between different proton species and the surface silica groups. The variation of the contact time in the HETCOR maps out different distance regimes (contact time of 3 ms: longer distances; contact time of 0.5 ms: shorter distances) and shows that both hydroxy- and aliphatic protons are in contact with the surface silicon nuclei. The result of the HETCOR is thus a snapshot of the liquid distribution inside the pores [162].

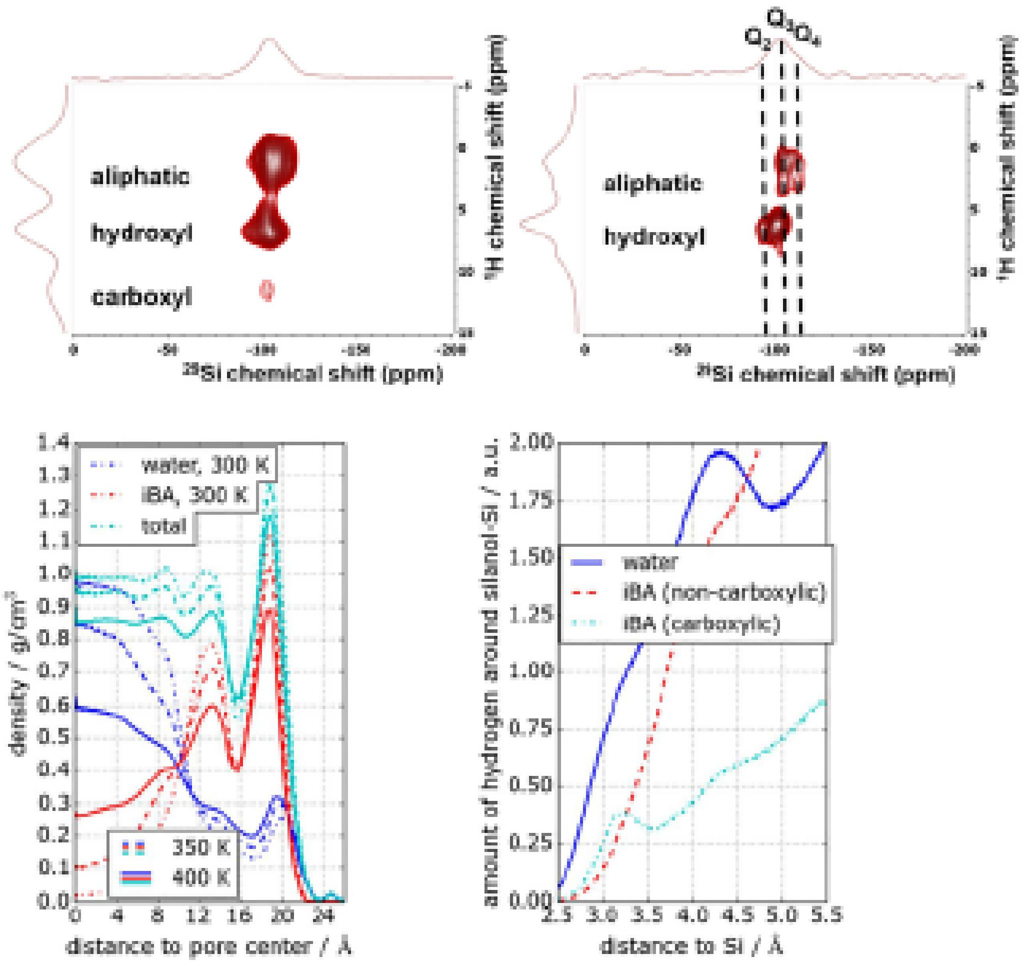

Figure 3: Upper row: 2D ^1H–^{29}Si FSLG HETCOR of iBA/H_2O mixtures (56 wt% iBA, 9.4 T, 110 K, 8 kHz MAS, 89 kHz FSLG homonuclear decoupling [163]) confined in SBA-15 (left: long contact time of 3 ms; right: short contact time of 0.5 ms). Lower row: MD simulations: left: density profiles for iBA and water (pore center at 0 Å; pore wall at 25 Å); right: hydrogen atom density as a function of the distance to the closest surface silanol group. The center of the pore is at 0 Å and the pore boundary is at 25 Å. (Figure adapted from Harrach et al. [162]).

The interpretation of these snapshots was performed by MD simulations (Figure 3, lower panel). The resulting density profiles of water and iBA as a function of the distance from the pore center corroborate the cylindrical model and assign the iBA rich phase to the outer cylinder and the water rich phase to the inner cylinder. In the outer cylinder the iBA molecules orient preferential like an inverted brush-like structure, where the carboxylic group interacts via hydrogen bonds with the silica surface and the aliphatic chains are oriented towards the pore-center [162]. The MD simulations revealed that the phase-behavior at low temperatures is mainly caused by the hydrogen-bonding enthalpy. Increasing the temperature causes a strengthening of entropic terms, which create stronger disorder and result in a higher miscibility.

3.3 Confined surfactants

In the next step, results on the behavior of nonionic surfactants doped with radicals confined in SBA-15 whose surface was modified with aminopropyltriethoxysilane are shortly summarized [164]. The samples were studied by a combination of DSC, SSNMR and Dynamic Nuclear Polarization (DNP) [77, 121, 165–167] enhanced SSNMR spectroscopy.

Figure 4 displays the temperature dependent ^{1}H-MAS-NMR spectra for bulk and confined $C_{10}E_6P_2$. The ^{1}H MAS spectra of the neat surfactants obtained at nominally 110 K were all observed to be extremely broad, indicating the presence of extensive dipolar proton–proton coupling. This is not too surprising as PEG and $C_{10}E_6P_2$ are saturated compounds and thus contain a large number of protons that become chemically non-equivalent due to molecular tumbling motions

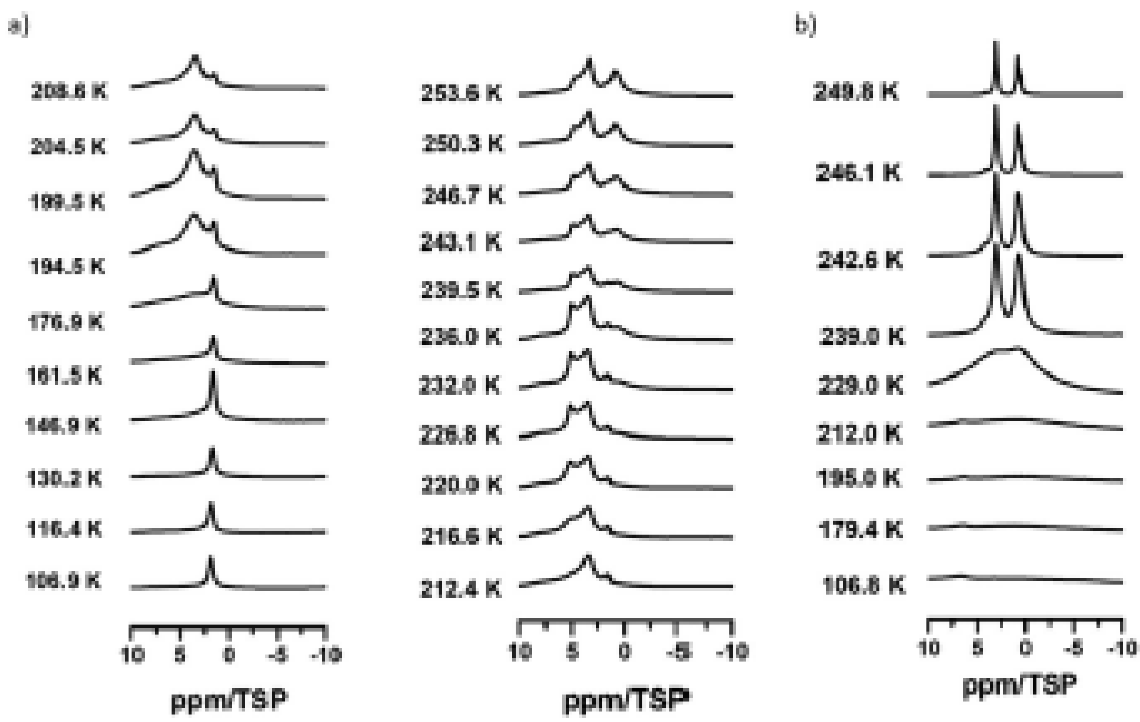

Figure 4: Temperature dependent ^{1}H MAS spectra of (a) $C_{10}E_6P_2$ confined in mesoporous silica material measured at 5 kHz spinning in the range between 106.9 K and 253.6 K; (b) neat $C_{10}E_6P_2$.

freezing out. The very broad ^{1}H MAS spectra do not allow any chemical differentiation of the protons. As can be seen from the spectra at higher temperatures the different functional groups of $C_{10}E_6P_2$ start their motions at different temperatures. When $C_{10}E_6P_2$ is confined in mesoporous silica, only one single signal and a very broad background signal (Figure 4(a)) is observable in the temperature regime below 176.9 K. This signal might refer to Si-OH, which rotates even at low temperature. When increasing the temperature, signals of the $C_{10}E_6P_2$ become visible and the melting of this surfactant starts stepwise indicating the different interactions of the various groups of the surfactant with the solid support material. The temperature dependent ^{1}H MAS spectra of pure $C_{10}E_6P_2$ (Figure 4(b)) display a different melting behavior. The motions of $C_{10}E_6P_2$ start at higher temperatures compared to the confined $C_{10}E_6P_2$. This proves that when mesoporous silica material is impregnated with $C_{10}E_6P_2$ the surfactant is indeed confined in the pores.

In parallel work, the Corzilius group and our group reported for the first time the observation of two superimposed resonance sets of opposite phase in low temperature DNP enhanced ^{13}C MAS NMR spectra of, respectively, peptide systems [168] and PEG related surfactants [169]. We will devote special attention in this review to this phenomenon as we believe it to be of importance in future DNP SSNMR investigations not only because it was observed later also in many other systems (see refs. [170, 171]) but also, as we will show, chemical insights might be gained from the details of the superimposed resonance sets. The experimental conditions were carefully explored in which theses superimposed resonance sets were present [169]. They were observed in all four investigated surfactants shown in Scheme 1 and three different radicals (two bi- and one mono-radical). As demonstrated for AMUPol in $C_{10}E_6$, larger radical concentration increases the broader upright resonance set compared to the inversely phased narrower resonance set. The scheme in Figure 5(c) explains the origin of the two resonance sets. They are created by two parallel polarization transfer paths, one direct path from electron spin to carbon nuclear spin represented by the broader lines, and one indirect path via the proton spin reservoir represented by the narrower lines. A detailed analysis shows that solid-state Nuclear Overhauser Effects (NOE)s [172] are responsible for the indirect pathway [168, 169]. While NOEs are commonly exploited in solution NMR, they are less frequently observed or applied in solid-state NMR owing to the lack of the necessary dynamics (see e.g. review by Haw for details [173]). The indirect pathway can be suppressed by 180° rotor-synchronized proton pulses as implemented in the pulse sequence shown in Figure 5(b).

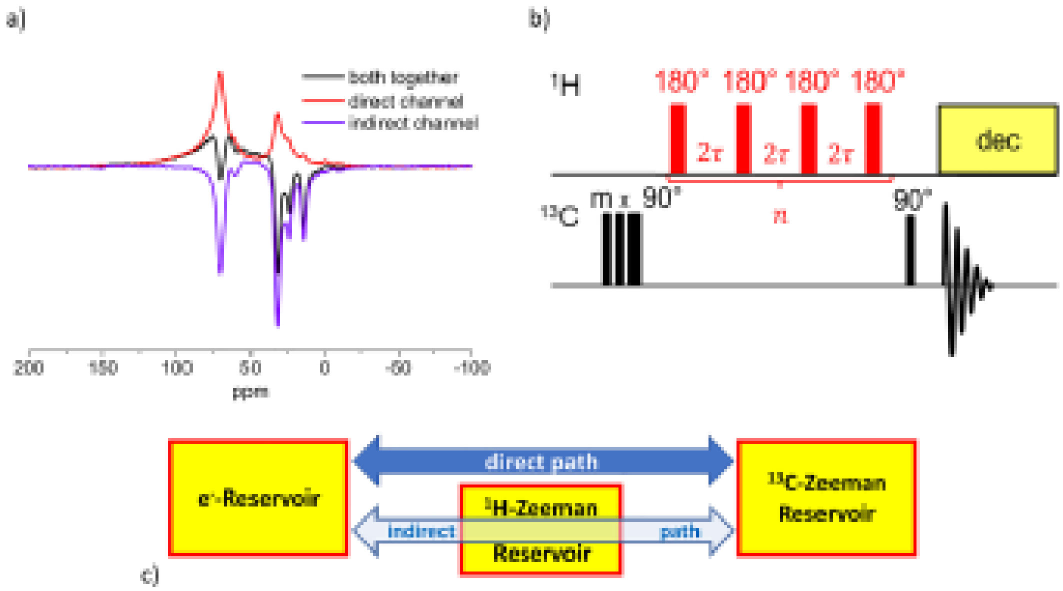

Figure 5: ^{13}C-DNP NMR: (a) DNP enhanced ^{13}C MAS NMR spectra of 20 mmol kg^{-1} AMUpol in $C_{10}E_6$: spectrum recorded without additional pulses (black line), with additional 180° pulses on ^{1}H (red line) representing the spectrum obtained via the direct channel, and difference spectrum of both, representing the spectrum obtained via the indirect channel (violet line). (b) Employed pulse sequence to suppress the indirect channel resonance (adapted from ref. [169]). (c) Cartoon of the different polarization transfer pathways.

Indirect polarization transfer through the proton spin reservoir requires the presence of molecular or intramolecular motions with correlation times sufficiently fast for modulating the heteronuclear dipolar interactions. Only the rotational hopping mode of methyl carbons has been known to provide such fast enough motional correlation times at the low experimental DNP temperature conditions of nominally 110 K [174, 175]. The astonishing aspect about the presence of the indirect path is that, in our work, the indirect path was also observed in PEG that does not possess methyl groups. This led us to further investigate this matter with additional experimentation where we could show the effect to be present also for organic solutes such as cyclohexane dissolved in the surfactant matrix [176]. An explanation was found through differential scanning calorimetry of the surfactant samples shown in Figure 6, which reveal significant differences between scanning rates of 10 vs 40 K/min. A cooling rate of 40 K/min approximates the cooling rate that the DNP NMR sample experiences when introduced from room temperature into the nominally 110 K cold NMR probe. From Figure 6, it can be seen that the sample cannot respond fast enough to such large cooling rates and experiences incomplete freezing processes. These relax during the heating cycle of the DSC as observed by the release of heat that causes the DSC response to be negative during heating. In the case of Triton X-100, there is even a large exothermic peak at ~240 K

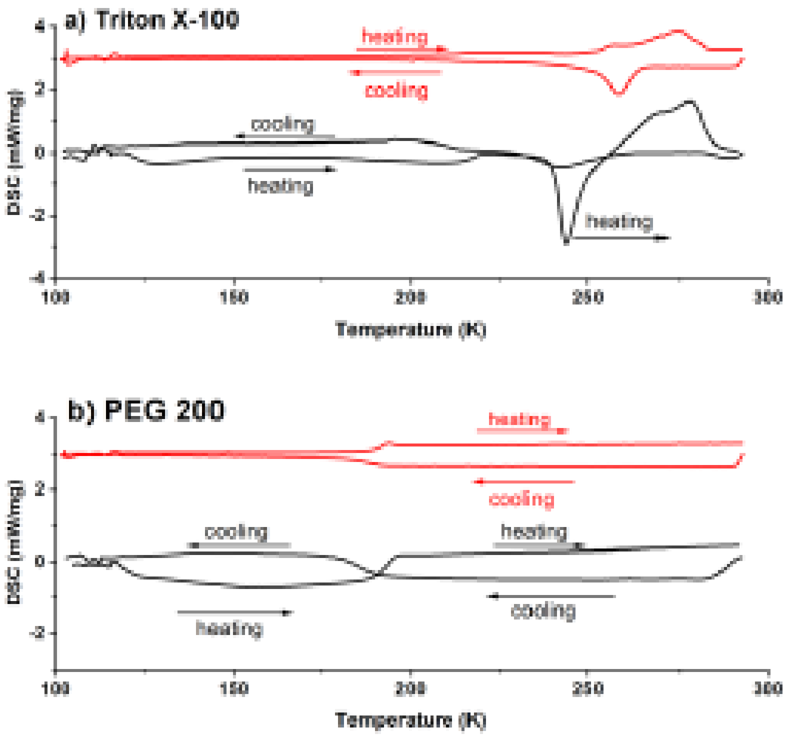

Figure 6: DSC scans of (a) Triton X-100, and (b) PEG 200 at cooling and heating rates of 10 K min^{-1} (red top traces) and 40 K min^{-1}(black bottom traces). The 10 K min^{-1} DSC scans are offset by +3 mW/mg to avoid clutter (adapted from ref. [176]).

observed during the heating cycle (Figure 6(a)). Evidently, the fast sample cooling experienced by the DNP leads to incomplete liquid to solid phase transitions resulting in a glass state or some other form of thermodynamic nonequilibrium state, with the unexpected consequence that some molecular motions are still active at DNP experimental low temperature conditions. This finding is of high importance to all researchers employing DNP because it may occur in a wide variety of samples.

The direct and indirect channel resonances in the DNP enhanced ^{13}C MAS spectra also display different magnetic field sweep enhancement profiles, or short enhancement profiles. We carefully explored the enhancement profiles of ^{1}H MAS, $^{1}H \rightarrow {}^{13}C$ CP MAS, and ^{13}C MAS direct and indirect channel resonances in a model study of AMUPol in $C_{10}E_6$ [177]. The normalized enhancement profiles of ^{1}H MAS, $^{1}H \rightarrow {}^{13}C$ cross polarization (CP) MAS, and ^{13}C MAS indirect channel resonances were all essentially identical (Figure 7) further confirming that the indirect channel resonances receive their DNP enhancement via the proton spin reservoir. Combined with the findings presented in ref. [169], the enhancement profiles also confirm that cross-effect (CE) is the operative DNP mechanism for the system of AMUPol in $C_{10}E_6$. Interestingly, while the shapes of the ^{13}C DNP enhancement profiles for $^{1}H \rightarrow {}^{13}C$ CP, direct and indirect channel ^{13}C signals were all found to be insensitive to the chemical nature of the carbon nuclei, their magnitudes reflected an ordering with respect to $C_{10}E_6$ structure increased from nonpolar alkyl chain to polar head group. This observation suggests a preferential orientation of the AMUPol radical towards the polar ethyl hydroxide head group of $C_{10}E_6$. This interpretation was further supported by independent T_1 relaxation measurements [176].

The simultaneous presence of direct and indirect channel resonances was also observed in 1,1,2,2-tetrachloroethane (TCE) for a series of novel biradicals [178]. It could be shown through DSC measurements and theoretical computations that those radicals with more flexible molecular structure would influence local motions of the TCE solvent and thus the occurrence of direct and indirect channel resonances. The occurrence of the direct and indirect channel resonance on ^{13}C-DNP depends on the flexibility of radicals in TCE (adapted from Bothe et al. [178]). Apparently, even the structural details of the polarizing agent play an important role for the indirect polarization transfer path to be active. In those cases where the host dynamics is of interest it is necessary to perform either MD-simulations as discussed or alternatively employ different concentrations of the radical and extrapolate back to zero radical concentration.

Next to the DNP studies of surfactants in their bulk phase, first preliminary DNP results were obtained for surfactants in confined environment, i.e., in the pores of APTES functionalized SBA material [164]. From the spectra for TOTAPOL in $C_{10}E_6$ shown in Figure 8(a) and (b), drastic differences are observed. Enhancement factors are reduced, and the line width becomes narrower for the ^{13}C direct channel. For $C_{10}E_6$ in bulk phase, the direct and indirect channel line widths are usually ca. 1.5–2 kHz and 700–800 Hz, respectively.

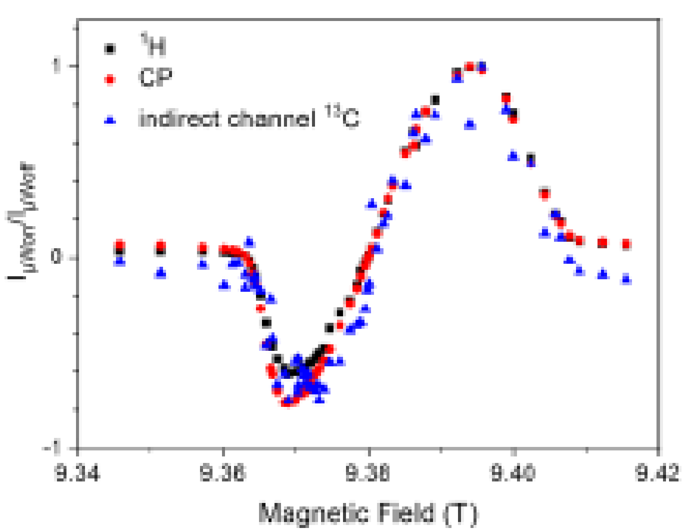

Figure 7: Normalized DNP enhancement profiles of 18 mmol kg^{-1} AMUPol in $C_{10}E_6$ for ^{1}H MAS (black squares), $^1H \rightarrow {}^{13}C$ CP MAS DNP (red circles) and the ^{13}C MAS indirect channel resonance (blue triangles). (Taken from ref. [177]).

In confinement, the line widths for both direct and indirect channel become equal, and the signals cancel each other out, if no 180° pulses on the proton channel are used as shown in Figure 8(b). Such cancelation of direct and indirect channel signals is not observed in the case of PEG 200 in SBA-APTES as shown in Figure 8(c). Here, it is interesting that one can observe the indirect channel signals from the APTES surface functionality besides the indirect channel signals from the PEG 200 solvent near 10, 25 and 45 ppm. In contrast, the APTES direct channel signals are barely observable compared to the PEG 200 solvent direct channel signals. Without DNP (MW off), the APTES functionalities are not discernible at all from the noise level with 512 scans. These exciting preliminary results warrant additional investigations to elucidate in how far factors such as pore size, choice of surfactant, radical and surface functionality affect the direct and indirect channel spectra. Potentially, structure – (spectral) property relationships might be revealed that conversely may then be utilized as a new investigative tool.

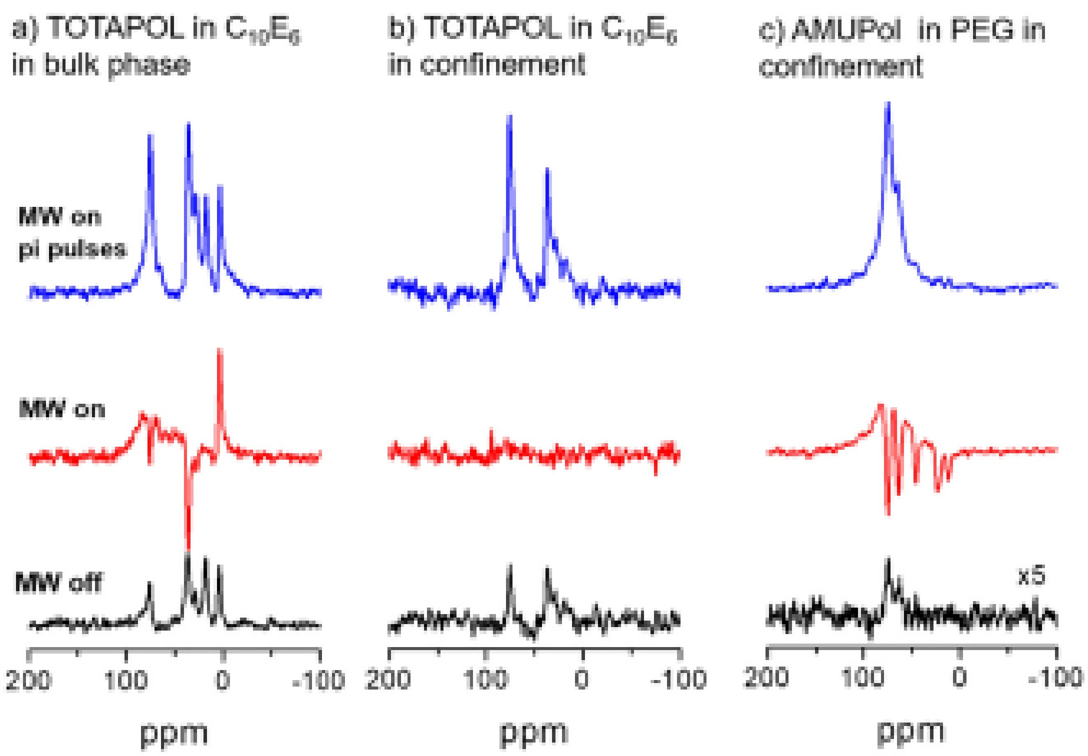

Figure 8: Comparison of ^{13}C MAS spectra obtained for (a) 15 mM TOTAPOL in $C_{10}E_6$ bulk phase, (b) 15 mM TOTAPOL in $C_{10}E_6$ in SBA-APTES confinement, and (c) 15 mM AMUPol in PEG 200 in SBA-APTES confinement. Spectra were recorded with MW on and MW off. Additional MW on spectra were recorded employing the sequence displayed in Figure 5(b), which suppresses indirect channel resonances (see Hoffmann et al. [164] for details).

4 Summary and outlook

This paper reviews recent advances to the characterization of small surfactants confined in microporous and mesoporous materials employing solid-state NMR techniques. It is shown that there is an exciting interplay between guest-guest and guest-host interactions, which changes the physicochemical properties of the confined surfactant. In DNP enhanced ^{13}C-SSNMR, an indirect hyperpolarization pathway was observed, which is related to a solid-state NOE effect, mediated via the proton Zeeman reservoir.

Author contribution: All the authors have accepted responsibility for the entire content of this submitted manuscript and approved submission.

Research funding: Financial support by the Deutsche Forschungsgemeinschaft in the framework of the Forschergruppe FOR 1583 through grants Bu-911/18-1/2, Bu-911/24-1/2, and the National Science Foundation [grant no 1953428] is gratefully acknowledged.

Conflict of interest statement: The authors declare no conflicts of interest regarding this article.

References

1. Mann S. *Biomineralization: Principles and Concepts in Bioinorganic Materials Chemistry*; Oxford University Press on Demand, 2001.
2. Hartmann M., Kostrov X. *Chem. Soc. Rev.* 2013, *42*, 6277.
3. Nassif N., Livage J. *Chem. Soc. Rev.* 2011, *40*, 849.
4. Vafaeezadeh M., Hashemi M. M. *J. Mol. Liq.* 2015, *207*, 73.
5. Han W., Liu C., Jin Z. *Adv. Synth. Catal.* 2008, *350*, 501.
6. Pires M., Purificação S., Santos A., Marques M. *Synthesis* 2017, *49*, 2337.
7. Khanmoradi M., Nikoorazm M., Ghorbani-Choghamarani A. *Catal. Lett.* 2017, *147*, 1114.
8. Buntkowsky G., Vogel M. *Molecules* 2020, *25*, 3311.
9. Buntkowsky G., Vogel M., Winter R. *Z. Phys. Chem.* 2018, *232*, 937.
10. Werner M., Rothermel N., Breitzke H., Gutmann T., Buntkowsky G. *Isr. J. Chem.* 2014, *54*, 60.
11. Fumagalli L., Esfandiar A., Fabregas R., Hu S., Ares P., Janardanan A., Yang Q., Radha B., Taniguchi T., Watanabe K., Gomila G., Novoselov K. S., Geim A. K. *Science* 2018, *360*, 1339.
12. Carvalho G., Paul E., Novais J. M., Pinheiro H. M. *Water Sci. Technol.* 2000, *42*, 135.
13. Hoffmann M. Nonionic Liquid Surfactants as Green Solvents. U.S. Patent, US20080097121A1, 2008.
14. Koganti V. R., Rankin S. E. *J. Phys. Chem. B* 2005, *109*, 3279.
15. Ramanathan M., Shrestha L. K., Mori T., Ji Q., Hill J. P., Ariga K. *Phys. Chem. Chem. Phys.* 2013, *15*, 10580.
16. Clark K. K., Keller A. A. *Water Air Soil Pollut.* 2012, *223*, 3647.

17. Le Page M., Beau R., Duchene J. Porous Silica Particles Containing a Crystallized Phase and Method. U.S. Patent US3493341A, 1970.
18. Chiola V., Ritsko J. E., Vanderpool C. D. Process for Producing Low-Bulk Density Silica. U.S. Patent US3556725A, 1970.
19. Vinu A., Hossain K. Z., Ariga K. *J. Nanosci. Nanotechnol.* 2005, *5*, 347.
20. Yokoi T., Yoshitake H., Tatsumi T. *J. Mater. Chem.* 2004, *14*, 951.
21. Wang X., Lin K. S. K., Chan J. C. C., Cheng S. *J. Phys. Chem. B* 2005, *109*, 1763.
22. Gedat E., Schreiber A., Albrecht J., Shenderovich I., Findenegg G., Limbach H.-H., Buntkowsky G., Buntkowsky G. *J. Phys. Chem. B* 2002, *106*, 1977.
23. Medick P., Blochowicz T., Vogel M., Roessler E. *J. Non-Cryst. Solids* 2002, *307*, 565.
24. Dosseh G., Xia Y., Alba-Simionesco C. *J. Phys. Chem. B* 2003, *107*, 6445.
25. Lusceac S. A., Koplin C., Medick P., Vogel M., Brodie-Linder N., LeQuellec C., Alba-Simionesco C., Roessler E. A. *J. Phys. Chem. B* 2004, *108*, 16601.
26. Alba-Simionesco C., Coasne B., Dosseh G., Dudziak G., Gubbins K. E., Radhakrishnan R., Sliwinska-Bartkowiak M. *J. Condens. Matter Phys.* 2006, *18*, R15.
27. Kiwilsza A., Pajzderska A., Gonzalez M. A., Mielcarek J., Wąsicki J. *J. Phys. Chem. C* 2015, *119*, 16578.
28. Krzyżak A. T., Habina I. *Microporous Mesoporous Mater.* 2016, *231*, 230.
29. Brilmayer R., Kübelbeck S., Khalil A., Brodrecht M., Kunz U., Kleebe H.-J., Buntkowsky G., Baier G., Andrieu-Brunsen A. *Adv. Mater. Interfaces* 2020, *7*, 1901914.
30. Beck J. S., Vartuli J. C., Roth W. J., Leonowicz M. E., Kresge C. T., Schmitt K. D., Chu C. T., Olson D. H., Sheppard E. W., McCullen S. B., Higgins J. B., Schlenker J. L. *J. Am. Chem. Soc.* 1992, *114*, 10834.
31. Zhao D. Y., Huo Q. S., Feng J. L., Chmelka B. F., Stucky G. D. *J. Am. Chem. Soc.* 1998, *120*, 6024.
32. Zhao D. Y., Feng J. L., Huo Q. S., Melosh N., Fredrickson G. H., Chmelka B. F., Stucky G. D. *Science* 1998, *279*, 548.
33. Nordberg M. E. *J. Am. Ceram. Soc.* 1944, *27*, 299.
34. Gelb L. D., Gubbins K. E., Radhakrishnan R., Sliwinska-Bartkowiak M. *Rep. Prog. Phys.* 1999, *62*, 1573.
35. Ciesla U., Schüth F. *Microporous Mesoporous Mater.* 1999, *27*, 131.
36. Brunauer S., Emmett P. H., Teller E. *J. Am. Chem. Soc.* 1938, *60*, 309.
37. Barrett E. P., Joyner L. G., Halenda P. P. *J. Am. Chem. Soc.* 1951, *73*, 373.
38. Treacy M. M. J., Higgins J. B., von Ballmoos R. *Collection of Simulated XRD Powder Patterns for Zeolites*; Elsevier: London, 1996.
39. Marler B., Oberhagemann U., Vortmann S., Gies H. *Microporous Mater.* 1996, *6*, 375.
40. Yao M. H., Baird R. J., Kunz F. W., Hoost T. E. *J. Catal.* 1997, *166*, 67.
41. Höhne G., Hemminger W. F., Flammersheim H.-J. *Differential Scanning Calorimetry*; Springer: Berlin Heidelberg, 2003.
42. Hemminger W. F., Cammenga H. K. *Methoden der thermischen Analyse*; Springer: Berlin, 1989.
43. Freude D., Kärger J. *Handbook of porous solids* 2002, *1*, 465.
44. Koller H., Weiß M. Solid state NMR of porous materials. In *Solid state NMR*; Springer, 2011, pp 189–227.
45. Haouas M., Martineau C., Taulelle F. Quadrupolar NMR of nanoporous materials. In *eMagRes*, 2011.
46. Kärger J. *ChemPhysChem* 2015, *16*, 24.
47. Thankamony A. S. L., Wittmann J. J., Kaushik M., Corzilius B. *Prog. NMR Spec.* 2017, 120–195.

48. Rankin A. G. M., Trébosc J., Pourpoint F., Amoureux J.-P., Lafon O. *Solid State NMR* 2019, *101*, 116.
49. Faivre C., Bellet D., Dolino G. *Eur. Phys. J. B* 1999, *7*, 19.
50. Alcoutlabi M., McKenna G. B. *J. Condens. Matter Phys.* 2005, *17*, R461.
51. Schoen M., Klapp S. *Rev. Comp. Chem.* 2007, *24*, 1.
52. Buntkowsky G., Breitzke H., Adamczyk A., Roelofs F., Emmler T., Gedat E., Grünberg B., Xu Y., Limbach H. H., Shenderovich I., Vyalikh A., Findenegg G. H. *Phys. Chem. Chem. Phys.* 2007, *9*, 4843.
53. Kärger J., Pfeifer H. *Zeolites* 1987, *7*, 90.
54. Kaerger J., Freude D. *Stud. Surf. Sci. Catal.* 1997, *105*, 551.
55. Kaerger J., Freude D. *Chem. Eng. Technol.* 2002, *25*, 769.
56. Freude D., Kärger J. *Handbook of porous solids* 2002, *1*, 465.
57. Kärger J., Freude D., Haase J. *Processes* 2018, *6*, 147.
58. Kaerger J., Valiullin R. *Chem. Soc. Rev.* 2013, *42*, 4172.
59. Findenegg G. H., Jaehnert S., Akcakayiran D., Schreiber A. *Chem. Phys. Chem.* 2008, *9*, 2651.
60. Geppi M., Borsacchi S., Mollica G., Veracini C. A. *Appl. Spectrosc. Rev.* 2009, 44, 1.
61. Vogel M. *Eur. Phys. J.* 2010, *189*, 47.
62. Yang Y., Beele B., Bluemel J. *J. Am. Chem. Soc.* 2008, *130*, 3771–+.
63. Bluemel J. *Coord. Chem. Rev.* 2008, *252*, 2410.
64. Gutmann T., Grünberg A., Rothermel N., Werner M., Srour M., Abdulhussain S., Tan S., Xu Y., Breitzke H., Buntkowsky G. *Solid State NMR* 2013, *55/56*, 1–11.
65. Motokura K., Itagaki S., Iwasawa Y., Miyaji A., Baba T. *Green Chem.* 2009, *11*, 1876.
66. Wang Q., Jordan E., Shantz D. F. *J. Phys. Chem. C* 2009, *113*, 18142.
67. Gath J., Hoaston G. L., Vold R. L., Berthoud R., Coperet C., Grellier M., Sabo-Etienne S., Lesage A., Emsley L. *Phys. Chem. Chem. Phys.* 2009, *11*, 6962.
68. Kandel K., Althaus S. M., Peeraphatdit C., Kobayashi T., Trewyn B. G., Pruski M., Slowing I. I. *J. Catal.* 2012, *291*, 63.
69. Kandel K., Althaus S. M., Peeraphatdit C., Kobayashi T., Trewyn B. G., Pruski M., Slowing I. I. *ACS Catal* 2013, *3*, 265.
70. Jayanthi S., Frydman V., Vega S. *J. Phys. Chem. B* 2012, *116*, 10398.
71. Sundaresan J., Werner M., Yeping X., Buntkowsky G., Vega S. *J Phys Chem C J Phys Chem C* 2013.
72. Jayanthi S., Kababya S., Schmidt A., Vega S. *J. Phys. Chem. C* 2016, *120*, 2797.
73. Saint-Arroman R. P., Chabanas M., Baudouin A., Coperet C., Basset J. H., Lesage A., Emsley L. *J. Am. Chem. Soc.* 2001, *123*, 3820.
74. Rataboul F., Chabanas M., de Mallmann A., Coperet C., Thivolle-Cazat J., Basset J. M. *Chem. Eur J.* 2003, *9*, 1426.
75. Blanc F., Basset J. M., Coperet C., Sinha A., Tonzetich Z. J., Schrock R. R., Solans-Monfort X., Clot E., Eisenstein O., Lesage A., Emsley L. *J. Am. Chem. Soc.* 2008, *130*, 5886.
76. Gajan D., Levine D., Zocher E., Coperet C., Lesage A., Emsley L. *Chem. Sci.* 2011, *2*, 928.
77. Lelli M., Gajan D., Lesage A., Caporini M. A., Vitzthum V., Mieville P., Heroguel F., Rascon F., Roussey A., Thieuleux C., Boualleg M., Veyre L., Bodenhausen G., Coperet C., Emsley L. *J. Am. Chem. Soc.* 2011, *133*, 2104–2107.
78. Kerber R. N., Kermagoret A., Callens E., Florian P., Massiot D., Lesage A., Coperet C., Delbecq F., Rozanska X., Sautet P. *J. Am. Chem. Soc.* 2012, *134*, 6767.
79. Valla M., Rossini A. J., Caillot M., Chizallet C., Raybaud P., Digne M., Chaumonnot A., Lesage A., Emsley L., van Bokhoven J. A., Coperet C. *J. Am. Chem. Soc.* 2015, *137*, 10710.

80. Conley M., Coperet C., Andersen R. *Abstr. Pap. Am. Chem. Soc.* 2016, 251.
81. Conley M. P., Lapadula G., Sanders K., Gajan D., Lesage A., Del Rosa I., Maron L., Lukens W. W., Coperet C., Andersen R. A. *J. Am. Chem. Soc.* 2016, *138*, 3831.
82. Delley M. F., Lapadula G., Nunez-Zarur F., Comas-Vives A., Kalendra V., Jeschke G., Baabe D., Walter M. D., Rossini A. J., Lesage A., Emsley L., Maury O., Coperet C. *J. Am. Chem. Soc.* 2017, *139*, 8855.
83. Estes D. P., Gordon C. P., Fedorov A., Liao W. C., Ehrhorn H., Bittner C., Zier M. L., Bockfeld D., Chan K. W., Eisenstein O., Raynaud C., Tamm M., Coperet C. *J. Am. Chem. Soc.* 2017, *139*, 17597.
84. Trebosc J., Wiench J. W., Huh S., Lin V. S. Y., Pruski M. *J. Am. Chem. Soc.* 2005, *127*, 7587.
85. Mao K., Pruski M. *J. Magn. Reson.* 2009, *201*, 165.
86. Mao K., Wiench J. W., Lin V., Pruski M. *J. Magn. Reson.* 2009, *196*, 92.
87. Hsin T. M., Chen S., Guo E., Tsai C. H., Pruski M., Lin V. *Top. Catal.* 2010, *53*, 746.
88. Mao K., Kobayashi T., Wiench J. W., Chen H. T., Tsai C. H., Lin V. S. Y., Pruski M. *J. Am. Chem. Soc.* 2010, *132*, 12452.
89. Kobayashi T., Mao K., Wang S. G., Lin V., Pruski M. *Solid State NMR* 2011, *39*, 65.
90. Hara K., Akahane S., Wiench J. W., Burgin B. R., Ishito N., Lin V. S. Y., Fukuoka A., Pruski M. *J. Phys. Chem. C* 2012, *116*, 7083.
91. Kobayashi T., Singappuli-Arachchige D., Wang Z. R., Slowing I. I., Pruski M. *Phys. Chem. Chem. Phys.* 2017, *19*, 1781.
92. Perras F., Kobayashi T., Pruski M. *Abstr. Pap. Am. Chem. Soc.* 2017, 253.
93. Kobayashi T., Singappuli-Arachchige D., Slowing I. I., Pruski M. *Phys. Chem. Chem. Phys.* 2018, *20*, 22203.
94. Kobayashi T., Pruski M. *ACS Catal* 2019, *9*, 7238.
95. Adamczyk A., Xu Y., Walaszek B., Roelofs F., Pery T., Pelzer K., Philippot K., Chaudret B., Limbach H. H., Breitzke H., Buntkowsky G. *Top. Catal.* 2008, *48*, 75.
96. Gutmann T., Ratajczyk T., Xu Y. P., Breitzke H., Grunberg A., Dillenberger S., Bommerich U., Trantzschel T., Bernarding J., Buntkowsky G. *Solid State NMR* 2010, *38*, 90.
97. Grunberg A., Gutmann T., Rothermel N., Xu Y. P., Breitzke H., Buntkowsky G. *Z. Phys. Chem.* 2013, *227*, 901.
98. Gutmann T., Grunberg A., Rothermel N., Werner M., Srour M., Abdulhussain S., Tan S. L., Xu Y. P., Breitzke H., Buntkowsky G. *Solid State NMR* 2013, *55–56*, 1.
99. Abdulhussain S., Breitzke H., Ratajczyk T., Grunberg A., Srour M., Arnaut D., Weidler H., Kunz U., Kleebe H. J., Bommerich U., Bernarding J., Gutmann T., Buntkowsky G. *Chem. Eur J.* 2014, *20*, 1159.
100. Gutmann T., Alkhagani S., Rothermel N., Limbach H. H., Breitzke H., Buntkowsky G. *Z. Phys. Chem.* 2017, *231*, 653.
101. Liu J. Q., Groszewicz P. B., Wen Q. B., Thankamony A. S. L., Zhang B., Kunz U., Sauer G., Xu Y. P., Gutmann T., Buntkowsky G. *J. Phys. Chem. C* 2017, *121*, 17409.
102. de Oliveira M., Seeburg D., Weiß J., Wohlrab S., Buntkowsky G., Bentrup U., Gutmann T. *Catal. Sci. Technol.* 2019, *9*, 6180.
103. de Oliveira M., Herr K., Brodrecht M., Haro-Mares N. B., Wissel T., Klimavicius V., Breitzke H., Gutmann T., Buntkowsky G. *Phys. Chem. Chem. Phys.* 2021, *23*, 12559.
104. Li Z., Rösler L., Wissel T., Breitzke H., Gutmann T., Buntkowsky G. *J. CO2 Util.* 2021, *52*, 101682.
105. Srour M., Hadjiali S., Brunnengräber K., Weidler H., Xu Y., Breitzke H., Gutmann T., Buntkowsky G. *J. Phys. Chem. C* 2021, *125*, 7178.

106. Folliet N., Gervais C., Costa D., Laurent G., Babonneau F., Stievano L., Lambert J.-F., Tielens F. *J. Phys. Chem. C* 2013, *117*, 4104.
107. Ukmar T., Cendak T., Mazaj M., Kaucic V., Mali G. *J. Phys. Chem. C* 2012, *116*, 2662.
108. Azaïs T., Laurent G., Panesar K., Nossov A., Guenneau F., Sanfeliu Cano C., Tourné-Péteilh C., Devoisselle J.-M., Babonneau F. *J. Phys. Chem. C* 2017, *121*, 26833.
109. Tielens F., Folliet N., Bondaz L., Etemovic S., Babonneau F., Gervais C., Azaïs T. *J. Phys. Chem. C* 2017, *121*, 17339.
110. Klimavicius V., Dagys L., Chizhik V., Balevicius V. *Appl. Magn. Reson.* 2017, *48*, 673.
111. Wu C., Guo F., Zhuang L., Ai X., Zhong F., Yang H., Qian J. *ACS Energy Lett* 2020, *5*, 1644.
112. Langer J., Epp V., Heitjans P., Mautner F. A., Wilkening M. *Phys. Rev. B* 2013, *88*, 094304.
113. Heitjans P. *Z. Phys. Chem.* 2015, *229*, 1263.
114. Wang Q., Sarkar A., Wang Di., Velasco L., Azmi R., Bhattacharya S. S., Bergfeldt T., Düvel A., Heitjans P., Brezesinski T., Hahn H., Breitung B. *Energy Environ. Sci.* 2019, *12*, 2433.
115. Heitjans P., Kärger J. *Diffusion in Condensed Matter: Methods, Materials, Models*, 3rd ed.; Springer: Berlin, 2018.
116. Ishii Y., Tycko R. *J. Magn. Reson.* 2000, *142*, 199.
117. Maly T., Debelouchina G. T., Bajaj V. S., Hu K., Joo C., Mak-Jurkauskas M. L., Sirigiri J. R., van der Wel P. C. A., Herzfeld J., Temkin R. J., Griffin R. G. *J. Chem. Phys.* 2008, *128*, 52211.
118. Hovav Y., Feintuch A., Vega S. *Phys. Chem. Chem. Phys.* 2013, *15*, 188.
119. Mentink-Vigier F., Akbey U., Hovav Y., Vega S., Oschkinat H., Feintuch A. *J. Magn. Reson.* 2012, *224*, 13.
120. Hovav Y., Feintuch A., Vega S. *J. Magn. Reson.* 2012, *214*, 29.
121. Lesage A., Lelli M., Gajan D., Caporini M. A., Vitzthum V., Mieville P., Alauzun J., Roussey A., Thieuleux C., Mehdi A., Bodenhausen G., Coperet C., Emsley L. *J. Am. Chem. Soc.* 2010, *132*, 15459.
122. Conley M. P., Drost R. M., Baffert M., Gajan D., Elsevier C., Franks W. T., Oschkinat H., Veyre L., Zagdoun A., Rossini A., Lelli M., Lesage A., Casano G., Ouari O., Tordo P., Emsley L., Coperet C., Thieuleux C. *Chem. Eur J.* 2013, *19*, 12234.
123. Conley M. P., Rossini A. J., Comas-Vives A., Valla M., Casano G., Ouari O., Tordo P., Lesage A., Emsley L., Coperet C. *Phys. Chem. Chem. Phys.* 2014, *16*, 17822.
124. Ong T. C., Liao W. C., Mougel V., Gajan D., Lesage A., Emsley L., Coperet C. *Angew. Chem. Int. Ed.* 2016, *55*, 4743.
125. Liao W. C., Ong T. C., Gajan D., Bernada F., Sauvee C., Yulikov M., Pucino M., Schowner R., Schwarzwalder M., Buchmeiser M. R., Jeschke G., Tordo P., Ouari O., Lesage A., Emsley L., Coperet C. *Chem. Sci.* 2017, *8*, 416.
126. Pump E., Bendjeriou-Sedjerari A., Viger-Gravel J., Gajan D., Scotto B., Samantaray M. K., Abou-Hamad E., Gurinov A., Almaksoud W., Cao Z., Lesage A., Cavallo L., Emsley L., Basset J. M. *Chem. Sci.* 2018, *9*, 4866.
127. Azais T., von Euw S., Ajili W., Auzoux-Bordenave S., Bertani P., Gajan D., Emsley L., Nassif N., Lesage A. *Solid State NMR* 2019, *102*, 2.
128. Eisenschmidt T. C., Kirss R. U., Deutsch P. P., Hommeltoft S. I., Eisenberg R., Bargon J., Lawler R. G., Balch A. L. *J. Am. Chem. Soc.* 1987, *109*, 8089.
129. Bowers C. R., Weitekamp D. P. *Phys. Rev. Lett.* 1986, *57*, 2645.
130. Bowers C. R., Jones D. H., Kurur N. D., Labinger J. A., Pravica M. G., Weitekamp D. P. *Adv. Magn. Res.* 1990, *15*, 269.
131. Hunger M. *Catal. Today* 2004, *97*, 3.
132. Henning H., Dyballa M., Scheibe M., Klemm E., Hunger M. *Chem. Phys. Lett.* 2013, *555*, 258.

133. Arzumanov S. S., Stepanov A. G. *J. Phys. Chem. C* 2013, *117*, 2888.
134. Buntkowsky G., Gutmann T., Petrova M. V., Ivanov K. L., Bommerich U., Plaumann M., Bernarding J. *Solid State NMR* 2014, *63-64*, 20.
135. Heinze M. T., Zill J. C., Matysik J., Einicke W. D., Gläser R., Stark A. *Phys. Chem. Chem. Phys.* 2014, *16*, 24359.
136. Fraissard J., Jameson C., Saam B., Brunner E., Hersman W., Goodson B., Meersmann T., Fujiwara H., Wang L.-Q., Sozzani P. *Hyperpolarized Xenon-129 Magnetic Resonance: Concepts, Production, Techniques and Applications*; Royal Society of Chemistry: London Cambridge, 2015.
137. Shantz D. F., Fild C., Koller H., Lobo R. F. *J. Phys. Chem. B* 1999, *103*, 10858.
138. Shantz D. F., Lobo R. F. *Top. Catal.* 1999, *9*, 1.
139. Wang B., Côté A. P., Furukawa H., O'Keeffe M., Yaghi O. M. *Nature* 2008, *453*, 207.
140. Riedel E., Janiak C. *Anorganische Chemie*; De Gruyter: Oldenburg, 2007.
141. Zhang C., Lively R. P., Zhang K., Johnson J. R., Karvan O., Koros W. J. *J. Phys. Chem. Lett.* 2012, *3*, 2130.
142. CEJKA J., van Bekkum H., Corma A., Schüth F. *Introduction to Zeolite Science and Practice, in Studies in Surface Science and Catalysis*, Vol. *168*; Elsevier BV: Amsterdam, Neth, 2007.
143. Demuth D., Sattig M., Steinrücken E., Weigler M., Vogel M. *Z. Phys. Chem.* 2018, *232*, 1059.
144. Kärger J., Vasenkov S., Auerbach S. M. Diffusion in zeolites. In *Handbook of Zeolite Science and Technology*; CRC Press, 2003, pp 458–560.
145. Weigler M., Brodrecht M., Breitzke H., Dietrich F., Sattig M., Buntkowsky G., Vogel M. *Z. Phys. Chem.* 2018, *232*, 1041.
146. Grünberg B., Emmler T., Gedat E., Shenderovich I., Findenegg G. H., Limbach H. H., Buntkowsky G. *Chem. Eur J.* 2004, *10*, 5689.
147. Brodrecht M., Breitzke H., Gutmann T., Buntkowsky G. *Chem. Eur J.* 2018, *24*, 17814.
148. Brodrecht M., Kumari B., Breitzke H., Gutmann T., Buntkowsky G. *Z. Phys. Chem.* 2018, *232*, 1127.
149. Brodrecht M., Kunnari B., Thankamony A. S. S. L., Breitzke H., Gutmann T., Buntkowsky G. *Chem. Eur J.* 2019, *25*, 5214.
150. Schottner S., Brodrecht M., Uhlein E., Dietz C., Breitzke H., Tietze A. A., Buntkowsky G., Gallei M. *Macromolecules* 2019, *52*, 2631.
151. Grün M., Unger K. K., Matsumoto A., Tsutsumi K. *Microporous Mesoporous Mater.* 1999, *27*, 207.
152. Buntkowsky G., Vogel M., Winter R. *Z. Phys. Chem.* 2018, *232*, 937.
153. Richert R. *Annu. Rev. Phys. Chem.* 2011, *62*, 65.
154. Brodrecht M., Klotz E., Lederle C., Breitzke H., Stühn B., Vogel M., Buntkowsky G. *Z. Phys. Chem.* 2018, *232*, 1003–1016.
155. Guo X.-Y., Watermann T., Sebastiani D. *J. Phys. Chem. B* 2014, *118*, 10207.
156. Hermens J. L., de Bruijn J. H., Brooke D. N. *Environ. Toxicol. Chem.* 2013, *32*, 732.
157. Leo A., Hansch C., Elkins D. *Chem. Rev.* 1971, *71*, 525.
158. Kumari B., Brodrecht M., Gutmann T., Breitzke H., Buntkowsky G. *Appl. Magn. Reson.* 2019, *50*, 1399.
159. Kumari B., Brodrecht M., Breitzke H., Werner M., Grunberg B., Limbach H. H., Forg S., Sanjon E. P., Drossel B., Gutmann T., Buntkowsky G. *J. Phys. Chem. C* 2018, *122*, 19540.
160. Vyalikh A., Emmler T., Shenderovich I., Zeng Y., Findenegg G. H., Buntkowsky G. *Phys. Chem. Chem. Phys.* 2007, *9*, 2249.

161. Vyalikh A., Emmler T., Gedat E., Shenderovich I., Findenegg G. H., Limbach H. H., Buntkowsky G. *Solid State NMR* 2005, *28*, 117.
162. Harrach M. F., Drossel B., Winschel W., Gutmann T., Buntkowsky G. *J. Phys. Chem. C* 2015, *119*, 28961.
163. van Rossum B. J., Förster H., de Groot H. J. M. *J. Magn. Reson.* 1997, *124*, 516.
164. Hoffmann M. M., Bothe S., Brodrecht M., Klimavicius V., Haro-Mares N. B., Gutmann T., Buntkowsky G. *J. Phys. Chem. C* 2020, *124*, 5145.
165. Hoffmann M. M., Bothe S., Gutmann T., Buntkowsky G. *J. Phys. Chem. B* 2018, *122*, 4913.
166. Hoffmann M. M., Too M. D., Vogel M., Gutmann T., Buntkowsky G. *J. Phys. Chem. B* 2020, *124*, 9115.
167. Hoffmann M. M., Horowitz R. H., Gutmann T., Buntkowsky G. *J. Chem. Eng. Data* 2021, *66*, 2480.
168. Daube D., Aladin V., Heiliger J., Wittmann J. J., Barthelmes D., Bengs C., Schwalbe H., Corzilius B. *J. Am. Chem. Soc.* 2016, *138*, 16572.
169. Hoffmann M. M., Bothe S., Gutmann T., Hartmann F.-F., Reggelin M., Buntkowsky G. *J. Phys. Chem. C* 2017, *121*, 2418.
170. Aladin V., Corzilius B. *Solid State NMR* 2019, *99*, 27.
171. Park H., Uluca-Yazgi B., Heumann S., Schlögl R., Granwehr J., Heise H., Schleker P. P. M. *J. Magn. Reson.* 2020, *312*, 106688.
172. Gibby M. G., Pines A., Waugh J. S. *Chem. Phys. Lett.* 1972, *16*, 296.
173. White J. L., Haw J. F. *J. Am. Chem. Soc.* 1990, *112*, 5896.
174. Macdonald P. M., Soong R. *J. Magn. Reson.* 2007, *188*, 1.
175. Higgins J. S., Hodgson A. H., Law R. V. *J. Mol. Struct.* 2002, *602–603*, 505.
176. Hoffmann M. M., Bothe S., Gutmann T., Buntkowsky G. *J. Phys. Chem. C* 2017, *121*, 22948.
177. Bothe S., Hoffmann M. M., Gutmann T., Buntkowsky G. *J. Phys. Chem. C* 2017, *121*, 27089.
178. Bothe S., Nowag J., Klimavičius V., Hoffmann M., Troitskaya T. I., Amosov E. V., Tormyshev V. M., Kirilyuk I., Taratayko A., Kuzhelev A., Parkhomenko D., Bagryanskaya E., Gutmann T., Buntkowsky G. *J. Phys. Chem. C* 2018, *122*, 11422.